Vector control of matrix converter-fed synchronous reluctance motor based on flux observer

# Vector Control of Matrix Converter-Fed Synchronous Reluctance Motor Based on Flux Observer

Arzhang Yousefi-talouki, and Gianmario Pellegrino, *Senior Member, IEEE*

***Abstract*-- In this paper, a synchronous reluctance motor fed by a matrix converter (MC) is current and flux controlled. Despite the advantages of matrix converters compared to conventional back-to-back converters, the application of these converters for synchronous reluctance motors (SyRMs) is not reported in the literature. The flux linkage on *d* axis and the current on *q* axis are closed loop controlled for the sake of a good combination of dynamic response and efficiency. Real-time maximum torque per Ampere usefully minimizes losses at all speeds, in particular at partial load. The input and output vectors of the converter are modulated using indirect space vector modulation technique. A flux observer provides the feedback to the *d* regulator. The nonlinearities of the converter are identified and compensated, to the benefit of voltage estimation and then flux estimation accuracy. Simulation results show that the presented MC-SyRM drive is promising for compactness and efficiency in critical applications.**

***Index Terms*-- Flux observer, Matrix converter, synchronous reluctance motor, Vector control**

## I. Introduction

Synchronous reluctance (SyR) motors offer several advantages, if compared to inverter driven ac motor counterparts [1-2]. Compared to induction motors, SyR motors provide higher efficiency at rated conditions due to absence of rotor cage losses [3]. Moreover, excitation flux of SyR motors can be real-time adjusted with load so to follow maximum torque per Ampere or maximum efficiency strategies. The same is not as simple for induction motors, because their rotor time constant would relent flux linkage regulation during torque transients [1]. Respect to permanent magnet (PM) machines, SyR motors are a low-cost solution due to the absence of permanent magnets, at the expense of a slightly lower torque density. Moreover, PM motors are penalized for their uncontrolled generator voltage in the case of unwilled inverter turn-off [4]. Therefore, SyR motors can provide higher safety in this respect, due to their natural de-excitation feature. Last, SyR motors do not propagate internal faults or winding short circuit faults after their supply is cut off, thanks again to their natural de-excitation attitude.

Dealing with matrix converters (MCs), these show attractive advantages such as controlled bidirectional power flow, sinusoidal input and output waveforms, elimination of bulky and life limited dc-link capacitors and therefore compact structure. [5-6]. The use of matrix converters is recently being consolidated in commercial applications such as aerospace actuators, marine propulsion, wind energy conversion, and electrical motor drives [7-12].

Despite the aforementioned advantages of MCs and SyR motors compared to the respective counterparts, the combination of MCs and SyR motors is not reported in the literature. In the authors' opinion, MC-SyRM drives can be competitive in those applications where compactness and efficiency are of importance, such as in aerospace actuators. Hence, this paper proposes the vector control of a matrix converter-fed synchronous reluctance motor. The control is based on the indirect space vector modulation technique. The *d* axis flux linkage and the current on *q* axis are closed-loop controlled through two proportional integral (PI) regulators. A flux observer is used in order to get a feedback for *d* regulator. As the nonlinearities of the converter lead to an inaccurate flux estimation, they are identified and compensated. The Maximum Torque per Ampere (MTPA) trajectory is used, as a simple way to obtain high efficiency at all load conditions and speed levels.

## II. Matrix Converter

The power circuit topology of a three-phase matrix converter is illustrated in Fig.1. The space vector of output voltages and input currents can be expressed as:

$$\overline{V_o} = \frac{2}{3}\left(V_a + V_b e^{j\frac{2\pi}{3}} + V_c e^{j\frac{-2\pi}{3}}\right) \quad (1)$$

$$\overline{I_i} = \frac{2}{3}\left(i_A + i_B e^{j\frac{2\pi}{3}} + i_C e^{j\frac{-2\pi}{3}}\right) \quad (2)$$

As illustrated in Fig.1, each of the three output phases can be connected to any of the input phases. In other words, for each output phase, there are three switching states. Therefore, there are $3^3 = 27$ potential switching states.

The authors are with the Politecnico di Torino, 10129 Turin, Italy (email: arzhang.yousefitalouki@polito.it; gianmario.pellegrino@polito.it )

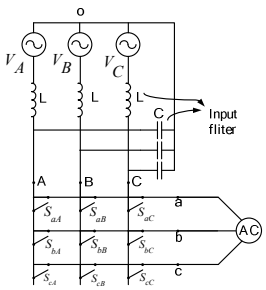


Fig.1: Schematic diagram of a three-phase matrix converter

### A. Indirect Space Vector Modulation (ISVM) [13]

The ISVM is used in this paper to synthesize the input current vector to the output voltage vector produced by PI-regulators. The basic idea under this modulation technique is to separate MC into a fictitious voltage source rectifier (VSR) plus a fictitious voltage source inverter (VSI), as illustrated in Fig.2. VSR is responsible for control of input current phase angle ($\theta_{in}^*$) and VSI is dedicated to output voltage modulation ($V_0^*$,$\theta_0^*$). Input and output sectors are determined according to the phase angles of measured input current and output voltage phase, respectively. Fig.3 shows an example for sector 1 for both input and output. The state of VSR defines the virtual *pn* rail. As an example, in Fig.3 (a) for sector 1, *pn* rail can be either $V_{AB}$, $V_{AC}$, or zero. On the other hand, as shown in Fig.3 (b), the output voltage of VSI can be either *pnn*, *ppn*, or zero. Combining VSI and VSR, there are five states: (*pnn*-$V_{AB}$, *pnn*-$V_{AC}$, *ppn*-$V_{AB}$, *ppn*-$V_{AC}$, and zero). For example, the state *pnn*-$V_{AB}$ means that output phase-*a* is connected to the input phase-*A*, and output phases *b* and *c* are connected to the input phase-*B*. Dealing with actual switches (Fig. 1), this situation is obtained with $S_{aA}$, $S_{bB}$ and $S_{cB}$ on. Thus in order to modulate the MC with ISVM, conventional SVM technique for VSRs and VSIs can be done and combined.

In both the VSR and VSI virtual stages, two adjacent vectors and one zero vector are used in order to produce a reference vector. The input and output active vector directions can be suitably defined as $\gamma, \delta$ for the VSR and $\mu, \nu$ for the VSI. The respective duty cycles are shown in Fig.3. Overall, modulation is obtained by the equivalent duty cycles:

$$d_{\mu\gamma} = d_\mu . d_\gamma = \frac{2}{\sqrt{3}} \frac{|V_0^*|}{|V_{in}|} sin\left(\frac{\pi}{3} - \theta_{in}^*\right) sin\left(\frac{\pi}{3} - \theta_0^*\right) \quad (3)$$

$$d_{\mu\delta} = d_\mu . d_\delta = \frac{2}{\sqrt{3}} \frac{|V_0^*|}{|V_{in}|} \sin(\theta_{in}^*) \sin\left(\frac{\pi}{3} - \theta_0^*\right) \quad (4)$$

$$d_{v\delta} = d_v . d_\delta = \frac{2}{\sqrt{3}} \frac{|V_0^*|}{|V_{in}|} \sin(\theta_{in}^*) \sin(\theta_0^*) \quad (5)$$

$$d_{v\gamma} = d_v . d_\gamma = \frac{2}{\sqrt{3}} \frac{|V_0^*|}{|V_{in}|} sin\left(\frac{\pi}{3} - \theta_{in}^*\right) sin(\theta_0^*) \quad (6)$$

$$d_0 = 1 - \left(d_{\mu\gamma} + d_{\mu\delta} + d_{v\delta} + d_{v\gamma}\right) \quad (7)$$

The amplitude of the reference output and input vectors are:

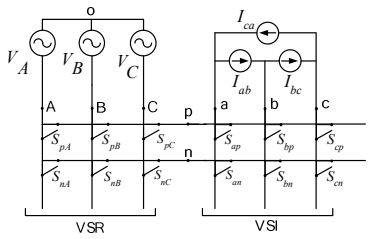


Fig.2: Emulation of VSR and VSI conversion

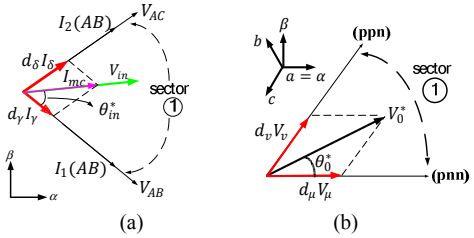


Fig.3: ISVM, (a) rectification space vector modulation, (b): inversion space vector modulation

$$|V_0^*| = \sqrt{(v_\alpha^*)^2 + (v_\beta^*)^2} \quad (8)$$

$$|V_{in}| = \sqrt{(V_{in,\alpha})^2 + (V_{in,\beta})^2} \quad (9)$$

The phase angles $\theta_{in}^*$ and $\theta_0^*$ depend on the sectors that their corresponding reference vectors lie.

## III. Vector Control of the SyR Machine

### A. Synchronous Reluctance Machine

The SyRM under investigation is a self-ventilated prototype rated 2.2 kW at 1500 rpm [3]. With reference to *dq* rotor frame, the model of the SyRM is:

$$v_{dq} = Ri_{dq} + j\omega\lambda_{dq} + \frac{d\lambda_{dq}}{dt} \quad (10)$$

$$\lambda_{dq} = \begin{bmatrix} L_d & 0 \\ 0 & L_q \end{bmatrix} i_{dq} \quad (11)$$

$$T = \frac{3}{2} p\left(\lambda_d i_q - \lambda_q i_d\right) \quad (12)$$

In the literature, most of known vector control techniques apply to SyRMs, including current vector control and direct torque control [14-15]. Very often, the simple magnetic model (11) is substituted with current to flux linkage relationships, in the form of look-up tables, to account for self- and cross-axis saturation effects. The magnetic curves of the machine under test are reported in Fig. 4.

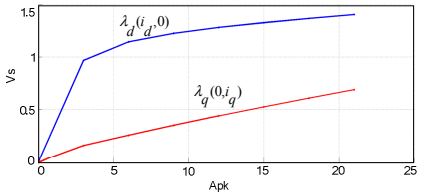


Fig.4: Current to flux linkage curves of the machine under test

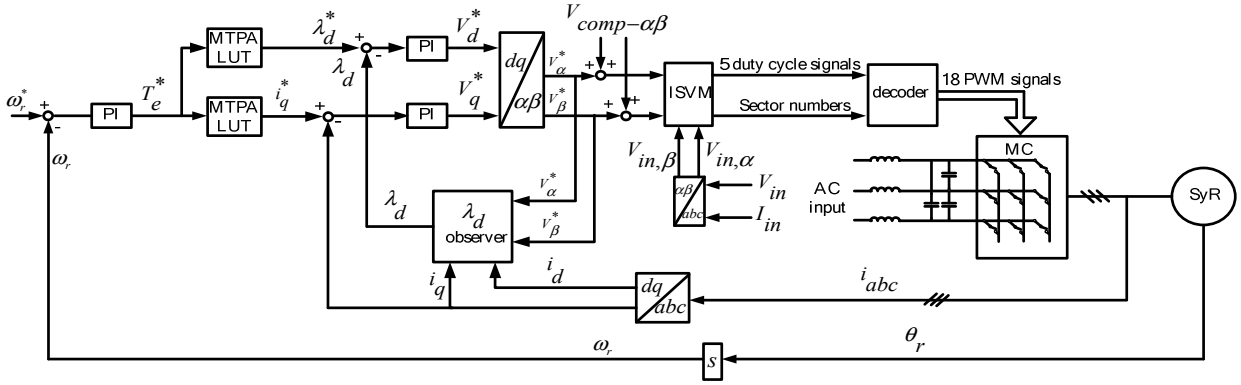


Fig5. Block diagram of the proposed control technique

### B. *Hybrid current and flux control*

Flux linkage on $d$ axis and current on $q$ axis are closed loop controlled. The proposed schematic diagram is depicted in Fig.5. The reference values of these variables $(\lambda_d^*, i_q^*)$ are determined by the torque reference through two maximum torque per ampere (MTPA) look-up tables (LUTs). The $d$ flux linkage is estimated using the flux observer described in Fig.6 [1]. Using the magnetic model of the motor, the flux linkage estimation is built $(\tilde{\lambda}_{\alpha\beta})$. This is used to build the observer feedback, make of flux linkage estimate error $(\tilde{\lambda}_{\alpha\beta} - \hat{\lambda}_{\alpha\beta})$ multiplied by the observer gain $G$ [rad/s].This gain sets the crossover speed between high speed model (back-EMF integral) and low speed model (LUTs). As the flux observer uses the voltage reference signals $(V_\alpha^*, V_\beta^*)$ as inputs, the nonlinearities of the converter lead to flux estimate errors. Hence, these nonlinearities should be compensated in an appropriate way. This issue is investigated in the next section.

## IV. NONLINEARITIES OF MATRIX CONVERTER

The two sources of voltage error in a MC are voltage drops (VD) of semiconductors and voltage edge uncertainty (EU) effect.

### A. *Voltage drop effect*

The voltage drop effects in a MC can be modeled with a simplified linearized model [16]. In MCs, two devices are always conducting. The forward voltage of a power device can be approximated by a fixed threshold value $(V_{th})$ which is the average effect of one diode and one IGBT. Thus, the VD is modeled as (13). $R_d$ accounts for two devices in series.

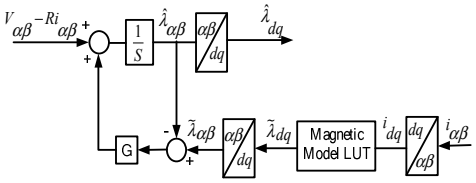


Fig.6. Block diagram of the flux observer

$$V_{Di} = 2V_{th} sign\,(I_i) + R_d I_i \;,\; i = \{a, b, c\} \tag{13}$$

### B. *Voltage Edge Uncertainty (EU) effect [17]*

A current-direction-based, four-step commutation scheme is considered in this paper. Also, a double-sided switching pattern [18] is used. Due to commutation, a voltage is introduced depending on commutation sequence and commutation pattern.

It is assumed that the input phase voltage lies in sector one (see Fig.7). The produced EU voltage error due to commutation is as (14), where $V_A$ is input voltage phase-$A$, $T_{pwm}$ is switching time, $t_c$ is commutation time, and $t_r$ and $t_f$ are IGBT rising and falling time, respectively. It can be seen from (14) that the extent of $V_{EU}$ depends on the input voltage phase-A. As depicted in Fig.7, $V_A$ varies in sector 1 between a minimum value $\frac{\sqrt{3}}{2}V_{pk}$ to a maximum value $V_{pk}$. Thus, the EU voltage error expressed in (14), varies between a maximum and minimum value, as illustrated in Fig.8. In the other sectors $V_A$ is replaced by one of the other two input voltages.

$$V_{EU\,i} = 3V_A \frac{t_c + t_f - t_r}{T_{pwm}}\, sign(I_i);\; i = \{a, b, c\} \tag{14}$$

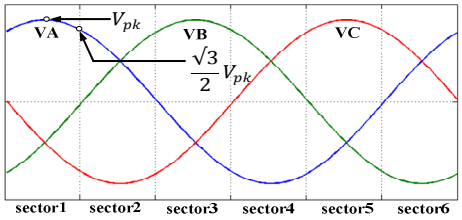


Fig.7: Input phase voltages and corresponding sectors

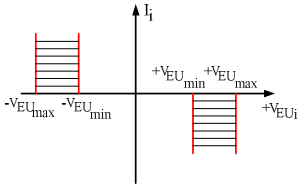


Fig.8: voltage edge uncertainty effect.

### C. Overall matrix converter error

It must be noticed that the two error sources described in previous subsections are opposite in sign. For positive current, the EU error adds to the output voltage, whereas the device voltage drop subtracts to, and vice versa for negative currents. Their combined effects give the total voltage error in MCs (15).

$$V_{error} = V_{Di} - 3V_j \frac{t_c + t_f - t_r}{T_{pwm}} \, sign(I_i) \quad (15)$$

$$j = \{A, B, C\}, \;\; i = \{a, b, c\}$$

The voltage error is defined $V_{error} = V_i^* - V_i$. It consists of linear and nonlinear parts. By substituting (13) in (15):

$$\Rightarrow V_{error} = V'_{th} sign(I_i) + R_d \, I_i \quad (16)$$

$$V'_{th}(6\vartheta_i) = 2V_{th} - 3V_j(6\vartheta_i) \frac{t_c + t_f - t_r}{T_{pwm}} \quad (17)$$

The equivalent threshold voltage $V'_{th}$ in (17) aggregates the EU and Vth effects, where $6\vartheta_i$ refers to the sector of input voltage. The device resistance $R_d$ is in series with the stator resistance $R_s$.

### D. Feedforward Compensation based on Signum Function

The MC voltage error (16) must be compensated in order to have an accurate flux estimation. The applied feedforward compensation scheme is depicted in Fig.9. Signum function based voltage errors are evaluated for the three output phases and then transformed into two-phase components αβ.

## V. Simulation Results

The motor and converter data is reported in Table I. Tests for two speed levels are presented: 10 rpm and 1500 rpm. Different load levels are compared, in terms of dynamic response and efficiency.

### A. SyRM control at 10 rpm

In this section motor is closed loop controlled at 10 rpm. At such low speed the converter errors are dominant. The effect of error compensation is investigated in this condition. The results show that without compensation the observed flux linkage is inaccurate and the torque control performance deteriorates.

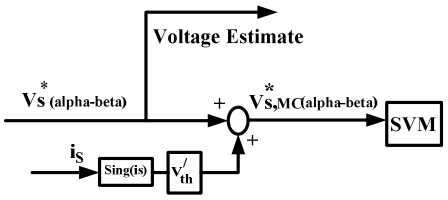


Fig.9: Feedforward compensation of MC voltage error

TABLE I
Matrix converter and SyR specification

| | |
|---|---|
| **SyR motor** | |
| Rated power/Number of poles | 2.2 kW / 6 |
| Nominal Speed/Rated Torque | 1500 rpm / 14 Nm |
| Stator resistance | 4.34 Ω |
| **Matrix Converter** | |
| EUPEC FM35R12KE3ENG module | |
| Switching device | 1200 V, 35 A, IGBT |
| $t_c$ | 0.2 $\mu s$ |
| $t_f$ / $t_r$ | 65-90 ns / 30-45 ns |
| power | 7.5 kW |
| AC input voltage | 3×415 V |

From t=0.5 [s] the speed increases to reach 10 rpm. First, converter nonlinearities are compensated. Also, it is assumed that motor is driven on no load condition up to t=3 [s]. In the period of t= [3-7 s], the load torque is 0.5 [N.m], and after that, load increases to 1 [N.m]. Electromagnetic torque, flux linkage on $d$ axis, and current on $q$ axis are depicted in Fig.10 (a, b and c), respectively. Fast dynamic behavior can be concluded from this figures. From Fig.10 (b), it is seen that the observed flux and actual one are very close to each other. As said, it is assumed that compensation process is enabled. It is shown in figures 11 (a) and (b) that there is no distortion and reference voltages in $(\alpha - \beta)$ frame are sinusoidal. Then, compensation technique is disabled. It can be seen from figures 12 (a) and (b) that the reference voltages are distorted due to converter errors. As the flux observer is based on these reference voltages, it is expected that an inaccurate flux observation is obtained. This fact is shown in Fig.13. As can be seen, the observed flux does not follow the actual flux linkage, with consequences on precision of torque set point (actual torque is larger than the controlled one in this test) and oscillation of flux linkage and torque at six time the frequency of the AC mains.

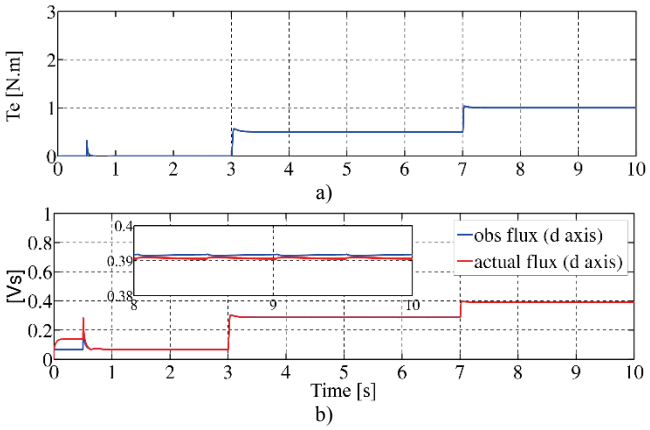

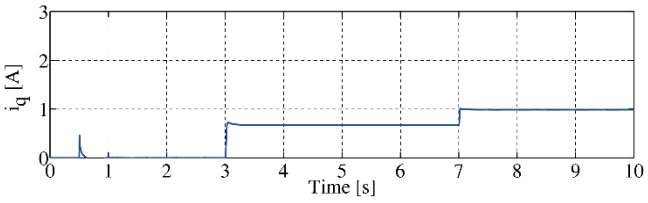


c)

Fig.10: Test at 10 rpm: a) motor torque; b) actual and observed *d* flux linkage; c) current on *q* axis.

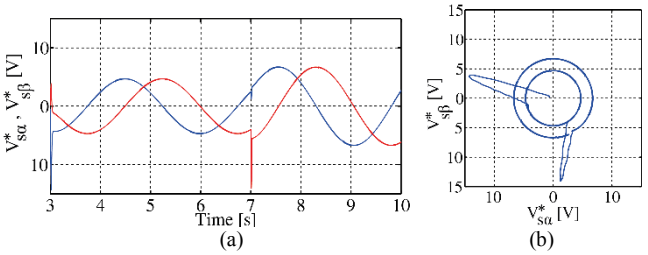


(a) (b)

Fig. 11. Reference voltages in (α-β) frame when MC error compensation is ON, at 10 rpm. a) (α-β) voltage waveforms; b) x-y representation of the same signal

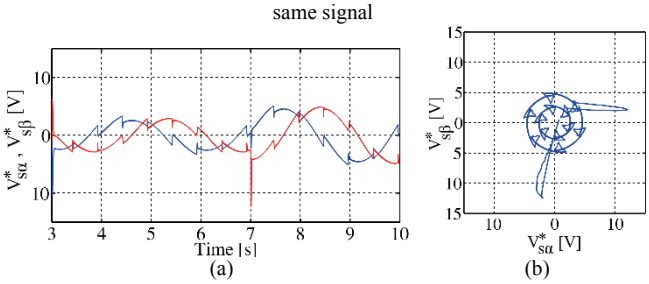


(a) (b)

Fig. 12. Reference voltages in (α-β) frame when MC compensation is OFF, at 10 rpm. a) ) (α-β) voltage waveforms; b) x-y representation of the same signal

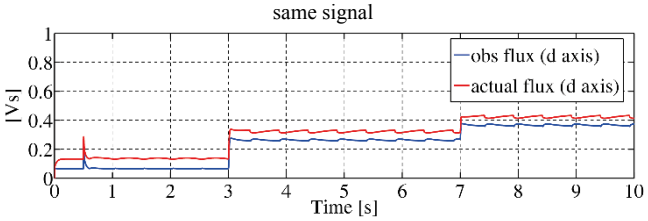


Fig.13: actual and observed flux on *d* axis when MC error compensation is OFF

## B. *Variable Load and Speed Test*

In this section the motor is controlled to follow a duty cycle including three torque load levels at 10 rpm and then at rated speed of 1500 rpm. The speed and load torque profiles are reported in Fig. 14, along with the stator voltage and current signals, in $\alpha\beta$ coordinates. As said, SyRM flux linkage and current are real-time adjusted with load to follow the MTPA trajectory. In turn, stator copper loss are inherently minimized at any load conditions.

$$P_{cu} = \frac{3}{2} R_s (i_\alpha^2 + i_\beta^2) \tag{18}$$

Moreover, flux linkage regulation with load also modulates core loss with load. A rough but significant estimate of fundamental iron loss in the machine is given by an equivalent resistance $R_{Fe}$ supplied by the motor back-emf. Therefore, at steady-state and disregarding the resistance voltage, core loss is approximately proportional to the square of the peak voltage:

$$P_{Fe} = \frac{3}{2} \frac{(\omega\lambda)^2}{R_{Fe}} \cong \frac{3}{2} \frac{(V_\alpha^2 + V_\beta^2)}{R_{Fe}} \tag{19}$$

It is evident in Fig. 14 that at zero torque the voltage is also close to zero, at rated speed, leading to negligible no load iron loss. At 5 Nm and 10 Nm the voltage grows progressively, and the core loss too. In turn, MTPA control and direct control of the *d*-axis flux linkage of the SyRM are a simple way to control the drive efficiency over the speed and torque operating range. This is possible thanks to the good dynamic response of the *d* flux linkage, typical of the SyRM. The same control strategy does not apply to induction motors or PMSM counterparts. In IMs the *d* axis excitation current is not varied with torque, below base speed, due to the poor dynamic response of *d* axis flux linkage. PMSMs, instead have the no load flux linkage hardly imposed by the PMs, producing iron loss at no load when the speed increases.

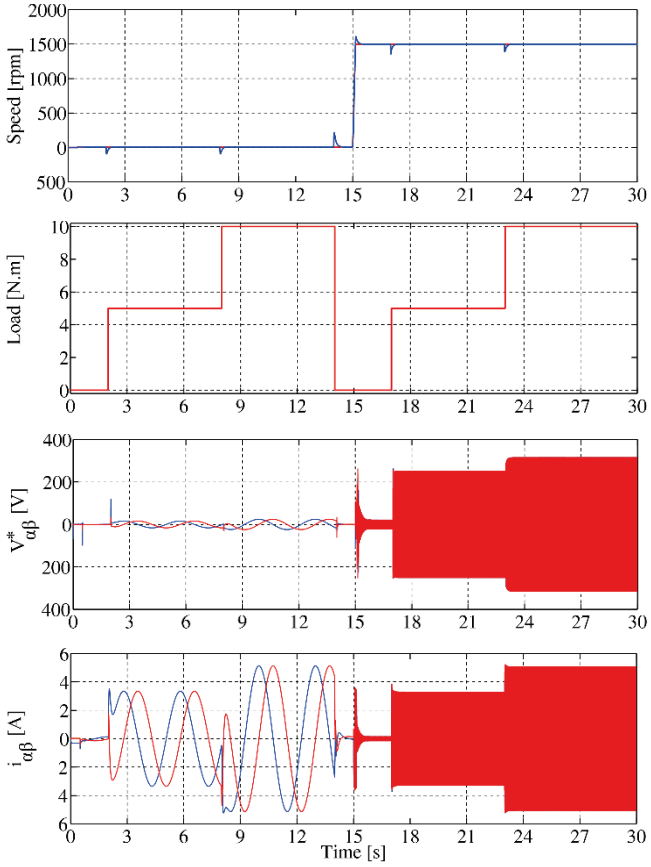


Fig.14: Duty-cycle including load torque from 0 to 0.71 p.u. at 10 rpm and rated speed

## VI. Conclusion

The paper proposes a MC supplied SyRM drive for high compactness and high efficiency applications. The converter is modulated using indirect space vector modulation . The hybrid flux and current vector controller is based on flux observer, requiring the knowledge of the machine model and the compensation of the converter voltage error. Fast MTPA control of the operating point guarantees good efficiency at all loads with a rather simple control scheme. Therefore, the MC-SyRM shows to be a promising solution for demanding applications.

## VII. References


[1] Vagati, A.; Pastorelli, M.; Franceschini, G., "High-performance control of synchronous reluctance motors," Industry Applications, IEEE Transactions on , vol.33, no.4, pp.983,991, Jul/Aug 1997.

[2] Vagati, A.; Pastorelli, M.; Francheschini, G.; Petrache, S.C., "Design of low-torque-ripple synchronous reluctance motors," Industry Applications, IEEE Transactions on , vol.34, no.4, pp.758,765, Jul/Aug 1998.

[3] Boglietti, A.; Cavagnino, A.; Pastorelli, M.; Vagati, A., "Experimental comparison of induction and synchronous reluctance motors performance," Industry Applications Conference, 2005. Fourtieth IAS Annual Meeting. Conference Record of the 2005 , vol.1, no., pp.474,479 Vol. 1, 2-6 Oct. 2005.

[4] Pellegrino, G.; Vagati, A.; Boazzo, B.; Guglielmi, P., "Comparison of Induction and PM Synchronous Motor Drives for EV Application Including Design Examples," Industry Applications, IEEE Transactions on , vol.48, no.6, pp.2322,2332, Nov.-Dec. 2012.

[5] Wheeler, P.W.; Rodriguez, J.; Clare, J.C.; Empringham, L.; Weinstein, A., "Matrix converters: a technology review," Industrial Electronics, IEEE Transactions on , vol.49, no.2, pp.276,288, Apr 2002.

[6] Rodriguez, J.; Rivera, M.; Kolar, J.W.; Wheeler, P.W., "A Review of Control and Modulation Methods for Matrix Converters," Industrial Electronics, IEEE Transactions on , vol.59, no.1, pp.58,70, Jan. 2012.

[7] Andreu, J.; Kortabarria, I.; Ormaetxea, E.; Ibarra, E.; Martin, J.L.; Apinaniz, S., "A Step Forward Towards the Development of Reliable Matrix Converters," Industrial Electronics, IEEE Transactions on , vol.59, no.1, pp.167,183, Jan. 2012.

[8] Xiaoyan Huang; Goodman, A.; Gerada, C.; Youtong Fang; Qinfen Lu, "A Single Sided Matrix Converter Drive for a Brushless DC Motor in Aerospace Applications," Industrial Electronics, IEEE Transactions on , vol.59, no.9, pp.3542,3552, Sept. 2012.

[9] Arias, A.; Silva, C.A.; Asher, G.M.; Clare, J.C.; Wheeler, P.W., "Use of a matrix converter to enhance the sensorless control of a surface-mount permanent-magnet AC motor at zero and low frequency," Industrial Electronics, IEEE Transactions on , vol.53, no.2, pp.440,449, April 2006.

[10] Dan Xiao; Rahman, M.F., "Sensorless Direct Torque and Flux Controlled IPM Synchronous Machine Fed by Matrix Converter Over a Wide Speed Range," Industrial Informatics, IEEE Transactions on , vol.9, no.4, pp.1855,1867, Nov. 2013.

[11] Imayavaramban, M.; Wheeler, P.W.; Clare, J.C., "Regeneration Control for Matrix Converter Drive," Industrial Electronics Society, 2007. IECON 2007. 33rd Annual Conference of the IEEE , vol., no., pp.1805,1810, 5-8 Nov. 2007.

[12] Yousefi-Talouki, A.; Pouresmaeil, E.; Jørgensen, B.N., "Active and reactive power ripple minimization in direct power control of matrix converter-fed DFIG," International Journal of Electrical Power & Energy Systems, Vol.63, pp. 600,608, Dec. 2014.

[13] Huber, L.; Borojevic, D., "Space vector modulated three-phase to three-phase matrix converter with input power factor correction," Industry Applications, IEEE Transactions on , vol.31, no.6, pp.1234,1246, Nov/Dec 1995.

[14] Malekian, K.; Sharif, M.R.; Milimonfared, J., "An optimal current vector control for synchronous reluctance motors incorporating field weakening," Advanced Motion Control, 2008. AMC '08. 10th IEEE International Workshop on , vol., no., pp.393,398, 26-28 March 2008.

[15] Zhang, X.N.; Foo, G.H.B.; Vilathgamuwa, D.M.; Maskell, D.L., "An Improved Robust Field Weakening Algorithm for Direct Torque Controlled Synchronous Reluctance Motor Drives," Industrial Electronics, IEEE Transactions on , vol.PP, no.99, pp.1,1.

[16] Kyo-Beum Lee; Blaabjerg, F., "A nonlinearity compensation method for a matrix converter drive," Power Electronics Letters, IEEE , vol.3, no.1, pp.19,23, March 2005.

[17] Arias, A.; Empringham, L.; Asher, G.M.; Wheeler, P.W.; Bland, M.; Apap, M.; Sumner, M.; Clare, J.C., "Elimination of Waveform Distortions in Matrix Converters Using a New Dual Compensation Method," Industrial Electronics, IEEE Transactions on , vol.54, no.4, pp.2079,2087, Aug. 2007.

[18] Casadei, D.; Serra, G.; Tani, A.; Zarri, L., "Matrix converter modulation strategies: a new general approach based on space-vector representation of the switch state," Industrial Electronics, IEEE Transactions on , vol.49, no.2, pp.370,381, Apr 2002.



**Arzhang Yousefi-Talouki** was born in Ghaemshahr, IRAN, in 1985. He received The M.Sc. degree in electrical engineering from Babol University of Technology, Babol, Iran in 2012. He is currently working toward the PhD degree in Politecnico di Torino, Turin Italy. His research interests include electrical machine drives.

**Gianmario Pellegrino,** is an Associate Professor with the Politecnico di Torino. He received the Ph.D. degree in electrical engineering from the same institution in 2002. His research interests include the design of electrical machines and the control of electrical drives. He is involved in research projects with industry and has several journal papers and one patent. Dr. Pellegrino is an Associate Editor for the IEEE Transactions on Industry Applications and an IEEE Senior Member. He is the co-recipient of three Prize Paper Awards. He was a guest researcher at Aalborg University, Denmark, in 2002, a visiting fellow at Nottingham University, UK, in 2010/2011, and an honorary fellow at the University of Wisconsin-Madison, USA, in 2013.